remote sensing

MDPI

Communication

A New Analysis Method for Magnetic Disturbances Possibly Related to Earthquakes Observed by Satellites

Xin-Yan Ouyang [1,*], Yong-Fu Wang [2], Xue-Min Zhang [1], Ya-Lu Wang [1] and Ying-Yan Wu [1]

[1] Institute of Earthquake Forecasting, China Earthquake Administration, Beijing 100036, China; zxm@ief.ac.cn (X.-M.Z.); wangyalu@ief.ac.cn (Y.-L.W.); wuyingyan@ief.ac.cn (Y.-Y.W.)
[2] School of Earth and Space Sciences, Peking University, Beijing 100871, China; wyffrank@pku.edu.cn
* Correspondence: oyxy@ief.ac.cn

Abstract: Studies on magnetic disturbances in ultralow frequency ranges related to earthquakes observed by satellites are still limited. Based on Swarm satellites, this paper proposes a new analysis method to investigate pre-earthquake magnetic disturbances by excluding some known non-earthquake magnetic effects that are not confined to those caused by intense geomagnetic activity. This method is demonstrated by two earthquake cases. One is an interplate earthquake, and the other is an intraplate earthquake. Magnetic disturbances around these two earthquakes are associated with solar wind and geomagnetic activity indices, electron density and field-aligned currents. Magnetic disturbances several days before earthquakes do not show clear relations with the already known magnetic effects. These nightside disturbances (LT~17/18, ~02), possibly related to earthquakes observed by Swarm satellites, oscillate in the transverse magnetic field below 2 Hz, propagate along the background magnetic field and are mostly linearly polarized.

Keywords: magnetic disturbances; earthquakes; plasma depletions; field-aligned currents; polarization parameters

Citation: Ouyang, X.-Y.; Wang, Y.-F.; Zhang, X.-M.; Wang, Y.-L.; Wu, Y.-Y. A New Analysis Method for Magnetic Disturbances Possibly Related to Earthquakes Observed by Satellites. *Remote Sens.* **2022**, *14*, 2709. https://doi.org/10.3390/rs14112709

Academic Editors: Kaiguang Zhu, Yunbin Yuan and Dedalo Marchetti

Received: 13 April 2022
Accepted: 31 May 2022
Published: 5 June 2022

1. Introduction

Electromagnetic variations associated with earthquakes have been reported in a wide range of frequencies from quasi-DC to very high frequency by ground or satellite observations. Electromagnetic disturbances in extremely low frequency (ELF, f < 3 kHz) or very low frequency (VLF, f < 30 kHz) ranges are extensively studied. Especially for VLF radio waves from ground-based transmitters, numerous studies have shown perturbations in the VLF phase and amplitude before earthquakes, e.g., [1,2]. Compared with ELF/VLF, electromagnetic observations in ultralow frequency (ULF, f < 10 Hz) are easier to obtain by both ground-based and space-based magnetometers. Furthermore, ground observations of electromagnetic disturbances in ULF are considered the most promising means for monitoring possible earthquake precursors because larger skin depths are comparable to the depths of hypocenters, e.g., [3]. A number of case and statistical studies based on ground observations have verified the existence of ULF electromagnetic disturbances, e.g., [4–8].

Theoretical calculations have shown that for an electromagnetic field of 0.01–100 Hz induced by seismic sources, only the fields from a magnetic type source can penetrate into the ionosphere and magnetosphere, and penetration is possible only in the ULF band (f < 10–20 Hz) [9]. Therefore, it is possible for ULF disturbances to be observed by satellites, which can offer widely covered and high-precision measurements. A few case studies have demonstrated anomalous electromagnetic signals in the ULF range before earthquakes observed by satellites, e.g., [10–13]. The most recent statistical study confirmed the association between earthquakes and ULF wave activity in the nighttime ionosphere [14]. It is common in pre-earthquake effect studies to use geomagnetic activity indices to exclude disturbances in the space environment. However, electromagnetic

disturbances in the ionosphere are affected by many energy sources other than intense geomagnetic activity. In addition, most previous studies on ULF disturbances related to earthquakes are based on the electric field in the DC/ULF band recorded by the DEMETER satellite [10–12,14,15]. However, only using electric field data limits further analyses of wave properties such as wave mode and polarization parameters. As a result, it becomes more difficult to deepen our understanding of ULF electromagnetic disturbances.

This study aims to investigate pre-earthquake ULF magnetic disturbances by excluding already known non-earthquake factors demonstrated by two different earthquake cases, interplate and intraplate earthquakes. It is hoped that this research will contribute to the practice of earthquake precursor analysis by analyzing magnetic field disturbances observed by satellites. Section 2 briefly describes the Swarm constellation and its data, as well as the main methods used in this paper. Section 3 presents magnetic field disturbances and their associations with solar wind and geomagnetic activity, electron density and field-aligned currents. The wave properties of magnetic field disturbances are also analyzed. Section 4 discusses the relationship between these disturbances and plasma depletions and midlatitude magnetic fluctuations. Section 5 summarizes our findings.

2. Data and Methods

Swarm is a low-Earth-orbiting constellation made up of three identical satellites: Alpha (A), Bravo (B) and Charlie (C). The three satellites were launched on 22 November 2013 to polar orbits at an ~87° inclination angle. Swarm A and C fly side-by-side at an initial altitude of ~460 km, and Swarm B cruises at a higher altitude of ~510 km. The main objective of Swarm is to measure the Earth's magnetic field. The vector field magnetometer (VFM) can provide three components of the magnetic field with sampling rates of 1 and 50 Hz. The Langmuir probe (LP) provides measurements of electron density and electron temperature at rates of 1 and 2 Hz. The Swarm level 2 FAC-dual product includes dual ionospheric radial currents (IRCs) and field-aligned currents (FACs) with a cadence of 1 Hz, which are produced per day and derived from the lower satellite pair Swarm A and C.

Three components of the magnetic field in North-East-Center (NEC) coordinates are transformed to local field-aligned coordinates (see Figure A1); these coordinates have three components in the radial (Br, toward outer L-shells), azimuthal (Ba, eastward) and parallel (Bp, parallel to the background magnetic field) directions. To highlight the magnetic disturbances, we apply a Savitzky–Golay smoothing filter [16] to define the trend of the magnetic field with a polynomial order of 2 and a frame length of 25 s·fs (sampling frequency). The residual magnetic field is obtained by subtracting the trend from the original magnetic field (see Figure A1c). A similar detrending method is used in studies on electromagnetic ion cyclotron waves, e.g., [17]. Polarization parameters (e.g., wave normal angle, ellipticity) are calculated by the methodology of Means [18,19] to study the possible origin and propagation characteristics of magnetic disturbances.

First, we choose magnetic data according to the estimated earthquake preparation area. Second, residual magnetic data are obtained by subtracting the background magnetic field, which is defined by the Savitzky–Golay smoothing filter. This method of obtaining the residual magnetic field has a faster running speed than subtracting the background magnetic field deduced from CHAOS. This detrending method with a faster processing speed is more convenient for the daily monitoring of magnetic disturbances possibly related to earthquakes. Third, the influences of solar wind and geomagnetic disturbances are excluded. Fourth, we analyze whether the remaining magnetic disturbances are related to significant plasma variations and intense FACs. If these magnetic disturbances are not closely connected with already-known main factors, we further investigate their wave properties.

3. Results

3.1. Overview of Magnetic Disturbances Observed by Swarm B

We show the results of an M7.7 earthquake case with a depth of 10 km that occurred at UTC 13:19:55 on 10 February 2021. The epicenter is located at 23.05°S and 171.66°E. This earthquake occurred as the result of low angle thrust faulting on or near the plate boundary interface between the Australia and Pacific plates. The location of this earthquake is close to the New Hebrides trench, where the Australia lithosphere converges with and sinks beneath the Pacific plate, descending into the mantle and forming the New Hebrides/Vanuatu subduction zone. This earthquake occurred on the subduction zone interface between the Australia and Pacific plates. (https://earthquake.usgs.gov/earthquakes/eventpage/us6000dg77/executive, (accessed on 13 May 2022)). According to Dobrovolsky's formula [20], it is known that the radius of the estimated earthquake preparation zone is approximately 2000 km, corresponding to an approximately 19° latitudinal range. Figure 1 shows the residual magnetic field variations observed by Swarm B in the range of 20° latitude by 20° longitude centered on the epicenter 15 days before and 7 days after the earthquake. The time range of our analysis is mainly based on previous studies on the time of pre-earthquake ionospheric effects, e.g., [14]. There are 39 orbits passing the area during this period and sometimes two orbits on the same day. The local time is approximately 16 or 17. Figure 1 presents the residual magnetic field recorded by each orbit, and it is known that clear magnetic disturbances appear in radial and azimuthal components on different days. As these magnetic disturbances may be affected by many factors, it is important to exclude some known causes. We will first analyze disturbances related to space weather events. Figure 2 provides the solar wind parameters and SYM-H index from 15 days before to 7 days after the earthquake, marked as day −15 to day 7. For the magnetic disturbances around day −15, SYM-H is less than −30 nT on day −15, with a recovery phase in the following days. Large amplitude and broad range disturbances, especially at higher latitudes, can be seen from orbits on day −15 and day −14, which suggests that these disturbances are affected by the weak magnetic storm on day −15 (SYM-H < −30 nT). In addition, there are two small jumps of dynamic pressure between day −9 and day −8 and between day −4 and day −3, followed by a small magnetic storm on day −3. Therefore, disturbances on day −9, day −8 and day −3 are eliminated from our study. Pulses on day −10 and day −2 shown in Figure 1a,b are not considered since they do not last long enough.

Figure 3a presents the remaining Swarm B orbits (LT~17) with magnetic disturbances in Br and Ba components after the above analysis, and Figure 3b–e show comparisons of these magnetic disturbances with the simultaneously measured electron density (Ne). There are no distinct perturbations in either the original or residual Ne.

3.2. Magnetic Disturbances Observed by Swarm A

Figure 4 shows observations from Swarm A at a similar local time (LT~18) and on the same day as that in Figure 3. We can see clear disturbances in the residual magnetic field in Br and Ba components in Figure 4b,c. Figure 4d,e present the original and residual Ne. In Figure 4e, residual Ne perturbations with a scale of 10^3 cm^{-3} can be seen from the orbit on day −12 at approximately −22° latitude and day −11 at approximately −15° latitude, which are simultaneous with magnetic disturbances in Br and Ba components. On other days, there are no clear perturbations in the residual Ne.

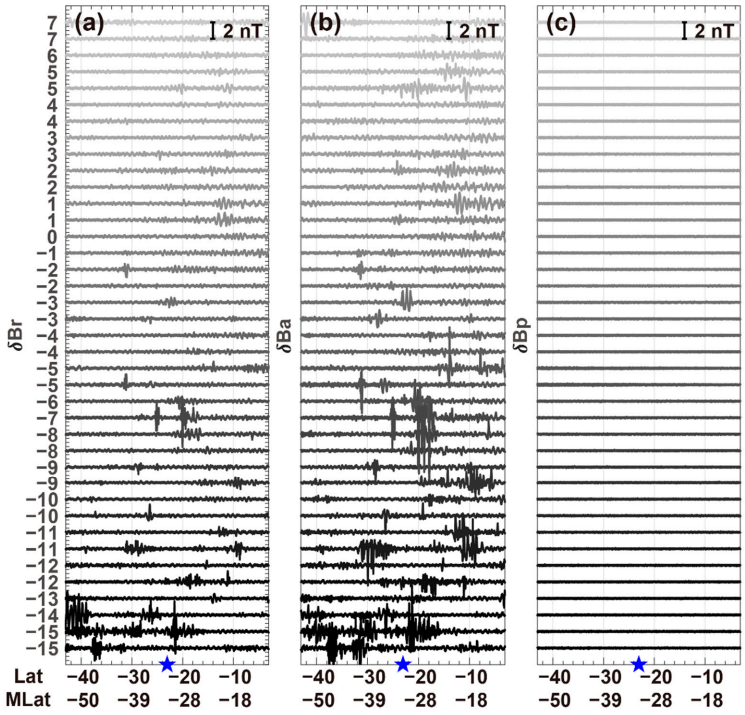

Figure 1. Magnetic disturbances observed by Swarm B 15 days before and 7 days after the M7.7 earthquake, and in the range of 20° latitude by 20° longitude centered on the M7.7 epicenter. (**a**–**c**) present the residual magnetic field in the radial, azimuthal and parallel directions. The stars on the horizontal axes indicate the epicenter's latitude, and the *y*-axis shows the time differences (ΔT in days) of each orbit relative to the day of the M7.7 earthquake.

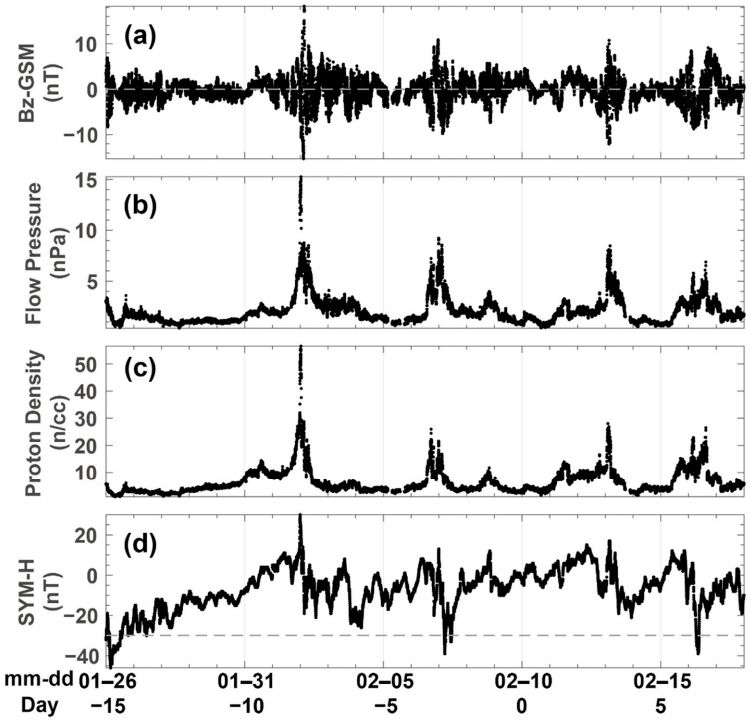

Figure 2. Solar wind parameters and SYM-H indices from 26 January to 17 February 2021, i.e., 15 days before to 7 days after the M7.7 earthquake. (**a**) IMF Bz in the GSM coordinate system, and the gray dashed line indicates Bz = 0; (**b**) the solar wind dynamic pressure; (**c**) the solar wind proton density; and (**d**) the SYM-H index. The gray dashed line indicates −30 nT.

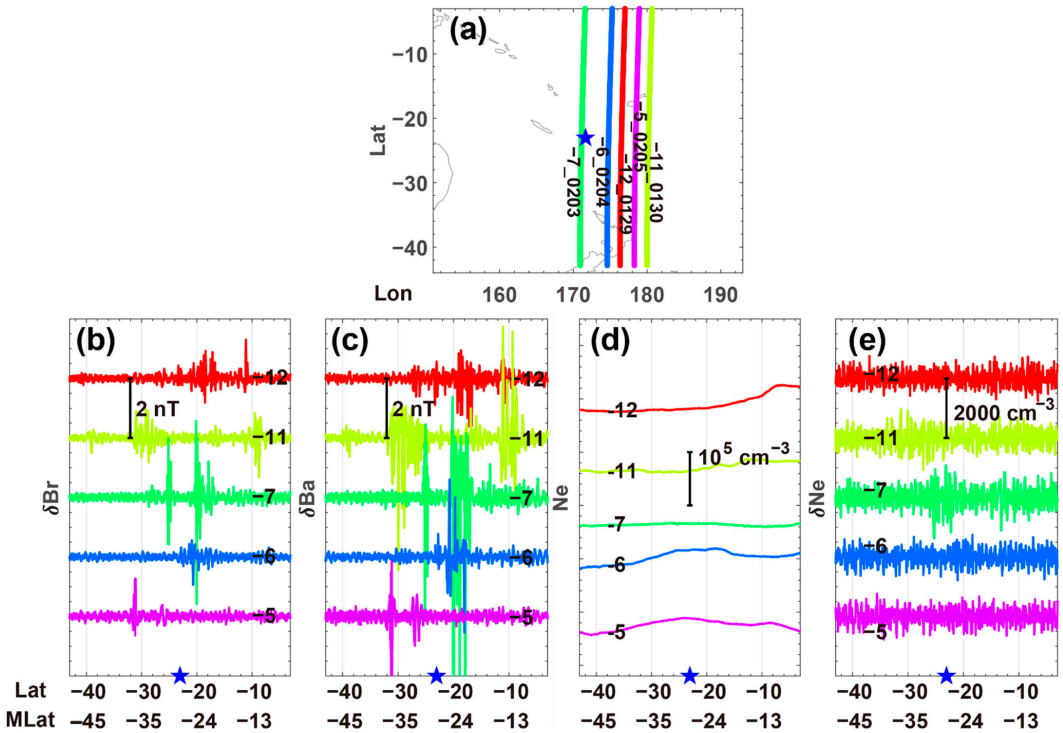

Figure 3. After removing the main influences of solar wind and SYM-H, a comparison between magnetic disturbances and electron density (Ne) was performed. (**a**) Swarm B orbits with magnetic disturbances (LT~17). The blue star indicates the epicenter. Numbers around orbits show time differences (ΔT in days) and the date of each orbit; (**b**,**c**) residual magnetic field in Br and Ba; (**d**) original Ne; (**e**) residual Ne.

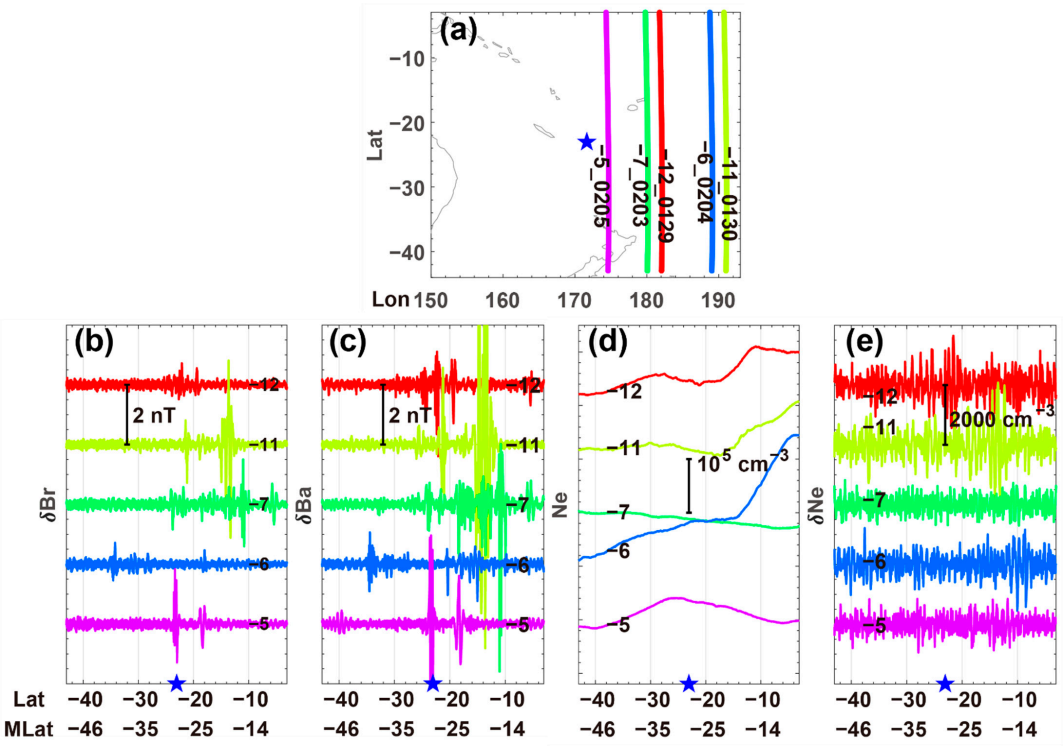

Figure 4. Observations from Swarm A at a similar local time (LT ~18) and on the same day as Swarm B orbits recorded magnetic disturbances. (**a**) Swarm A orbits; the blue star indicates the epicenter; (**b**,**c**) residual magnetic field in Br and Ba; (**d**) original Ne; (**e**) residual Ne.

3.3. Relationship with Field-Aligned Currents (FACs)

This section shows FACs in the area of 20° latitude by 20° longitude centered on the epicenter. Since the FAC deduced from single-satellite magnetic field data needs to make a number of assumptions, we use more realistic FACs computed from the lower satellite pair Swarm A and C (Swarm Level 2 FAC-dual product) [21,22]. Figure 5 presents tracks and FACs in this area on disturbed days −12, −11, −7, −6 and −5. Although the tracks in Figure 5a do not completely correspond to the orbits of Swarm A in Figure 4, we show FACs in the same area of interest that can be used as a reference. From Figures 3a and 4a, it is known that the disturbed orbits are mainly around the east side of the epicenter, and the right tracks in Figure 5a may give reference FACs for these disturbed orbits. Figure 5g–k show FACs along the right overlapped tracks, and variations in FACs are almost the same on different disturbed days. A comparison of Figure 5a with Figure 4a shows that the orbit on day −12 in Figure 4a is the closest to the right tracks in Figure 5a. We can see magnetic disturbances with larger amplitudes in δBa on day −12 above the epicenter in Figure 4c. Figure 5g shows FACs on day -12, and they have values of zero to median above the epicenter. From Figure 5, it is known that FACs are very weak, changing around the median FACs and mostly within 0.04 μA/m^2.

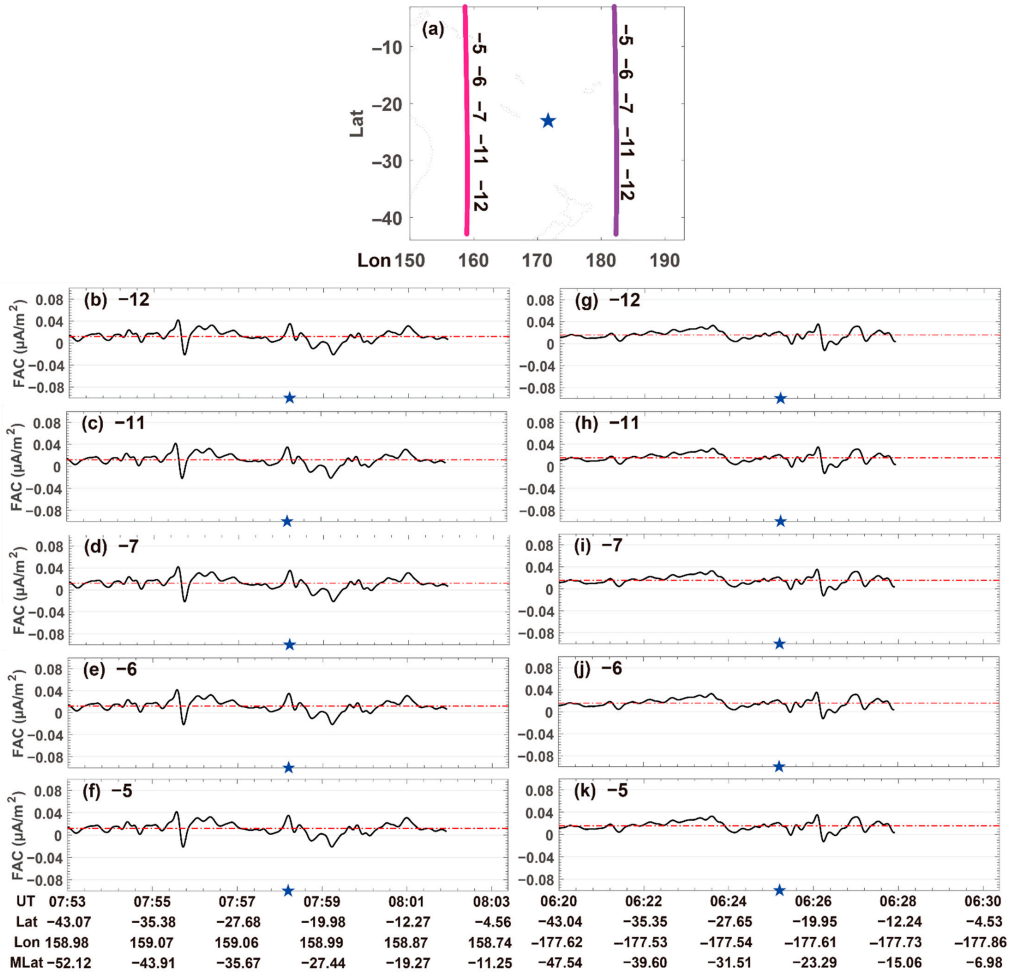

Figure 5. Field-aligned currents (FACs) in the range of 20° latitude by 20° longitude centered on the M7.7 epicenter on the disturbed days. (**a**) Tracks in this area; the blue star shows the epicenter; (**b**–**f**) FACs on days −12, −11, −7, −6 and −5 along the left tracks in (**a**); (**g**–**k**) FACs on days −12, −11, −7, −6 and −5 along the right tracks in (**a**). The blue star indicates the epicenter's latitude, and the red dashed lines represent the median FACs along the corresponding tracks in the area of interest.

3.4. Analysis of Polarization Parameters

Since these magnetic disturbances do not have a clear relationship with FACs, further analysis of wave properties is presented. Figures 6 and 7 show the power spectral density and polarization parameters of Swarm B and A orbits in Figures 3 and 4, respectively. These disturbances are located below 2 Hz, and they oscillate in the perpendicular magnetic field (Br and Ba components). Combined with polarization parameters, we know that these disturbances propagate along the background magnetic field and are mostly linearly polarized.

3.5. An Intraplate Earthquake Case Study

In this section, we show magnetic disturbances of an M7.0 earthquake case with a depth of 21 km that occurred at UTC 11:51:27 on 30 October 2020. This earthquake is located at 37.90°N, 26.78°E, and is considered an intraplate event as the result of normal faulting at a shallow crustal depth within the Eurasia tectonic plate (https://earthquake.usgs.gov/earthquakes/eventpage/us7000c7y0/executive, (accessed on 13 May 2022)). The analysis method described in the above section is applied to this earthquake. The radius of the estimated preparation area is about 1000 km, around 10° latitudinal range. Figure 8 presents residual magnetic field 15 days before and 7 days after the earthquake. There are no orbits at 7 days after the earthquake when the range is limited to 10° latitude by 10° longitude centered on the epicenter. Magnetic disturbances in Br and Ba components occurred at ΔT = −8, −3 and −1 days. Combined with solar wind parameters and SYM-H indices in Figure 9, we know that above magnetic disturbances are not influenced by space weather events. Similar to the analysis of the M7.7 earthquake, these magnetic disturbances are related to simultaneous electron density (see Figure A2) and referenced FACs at similar local times (see Figure A3). Their correlations are not found. At last, we further analyze power spectral density and polarization parameters for these disturbances (see Figure A4).

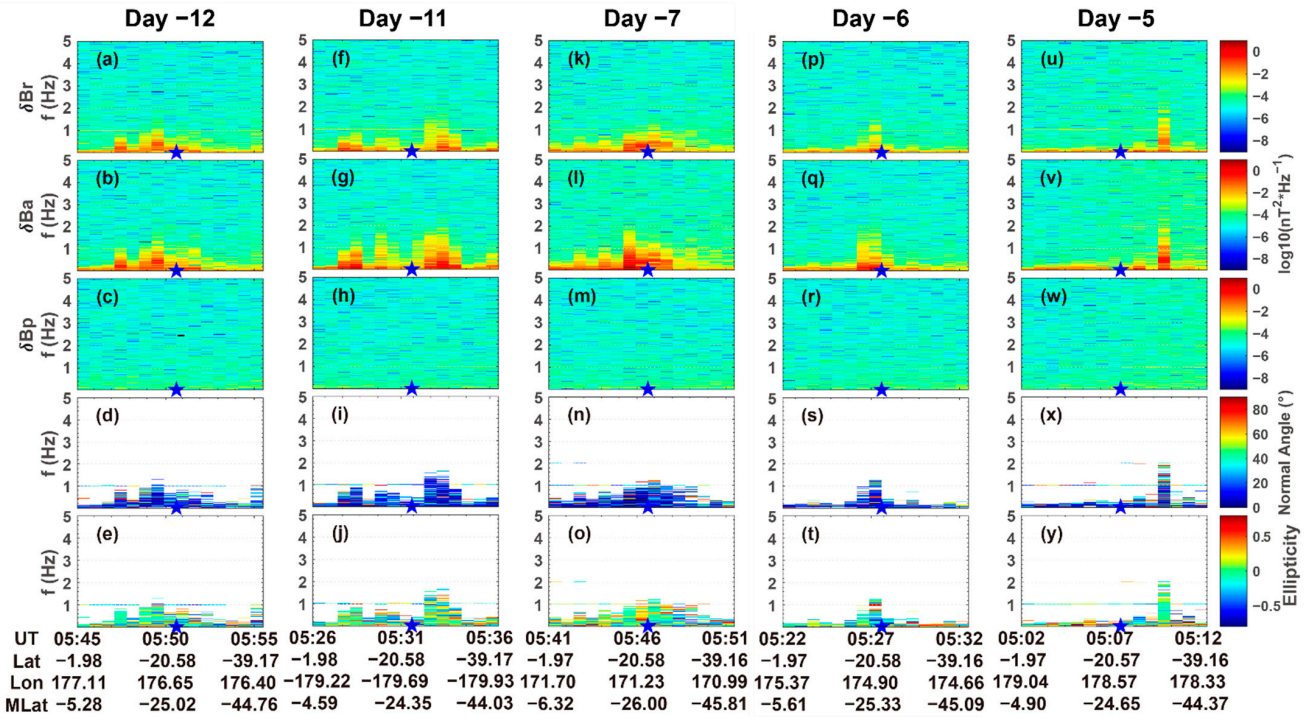

Figure 6. Power spectral density and polarization parameters corresponding to Swarm B orbits in Figure 3. Different columns represent different orbits. For example, the first column shows the power spectral density in panels (**a**–**c**), as well as the wave normal angle and ellipticity in panels (**d**,**e**) on day −12. The second to fifth columns (**f**–**y**) show the power spectral density and polarization parameters on days −11, −7, −6 and −5. The blue star indicates the epicenter.

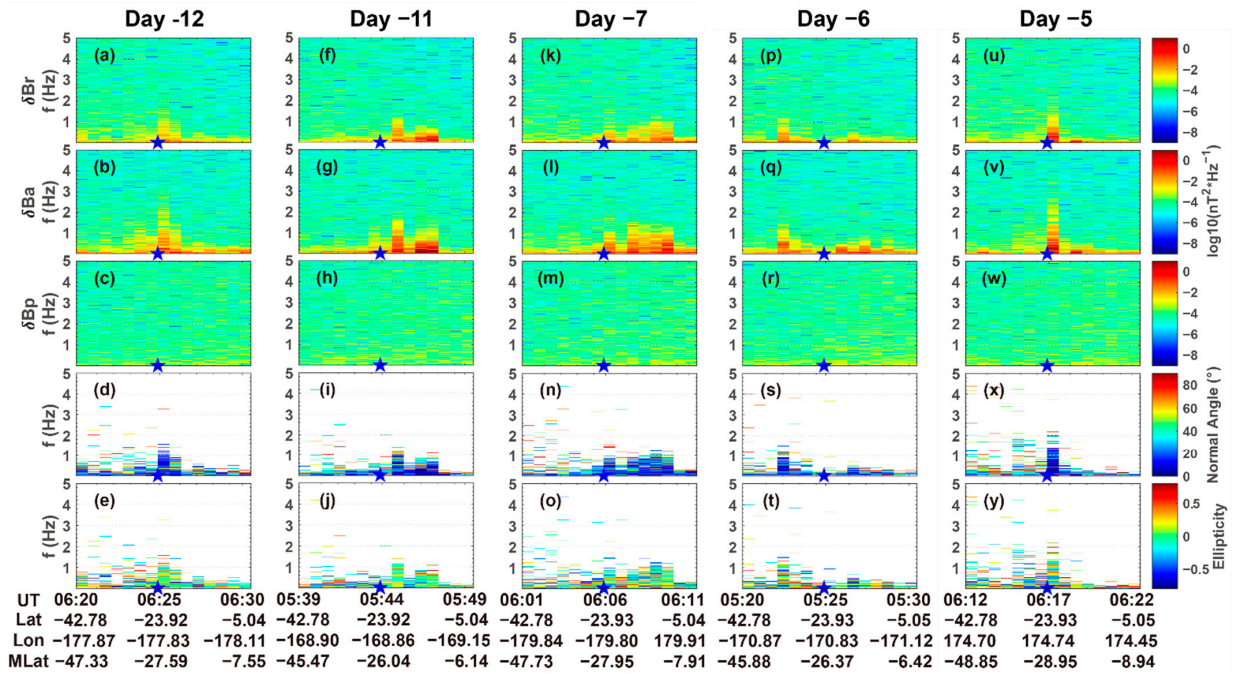

Figure 7. Power spectral density and polarization parameters corresponding to Swarm A orbits shown in Figure 4. The first to the fifth columns show the power spectral density (the first three rows (**a**–**c**,**f**–**h**,**k**–**m**,**p**–**r**,**u**–**w**)) and polarization parameters (the fourth and the fifth rows (**d**,**e**,**i**,**j**,**n**,**o**,**s**,**t**,**x**,**y**)) on days −12, −11, −7, −6 and −5. The blue star indicates the epicenter.

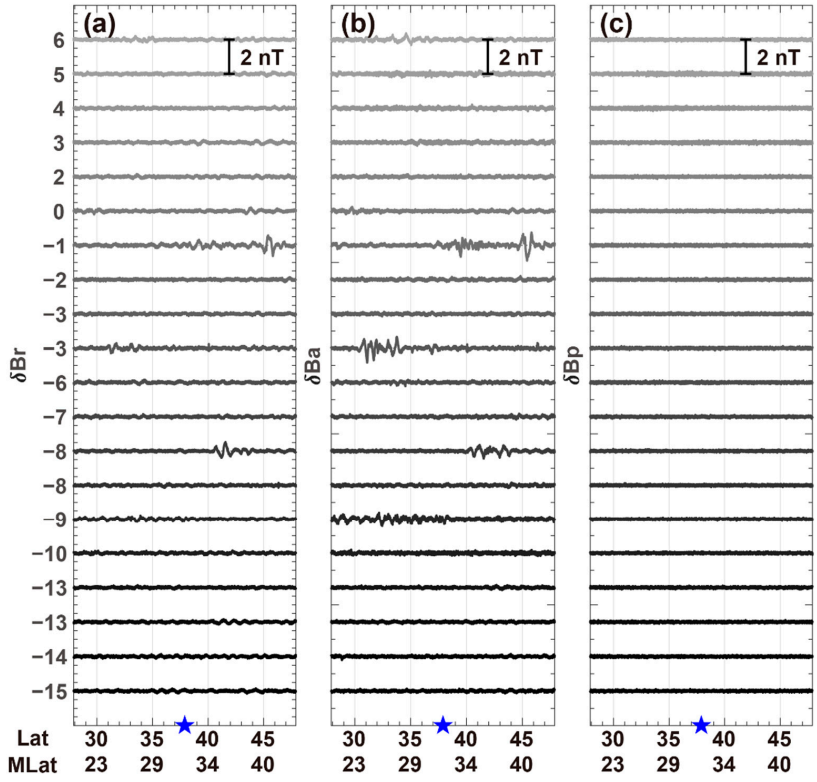

Figure 8. Magnetic disturbances observed by Swarm B 15 days before and 7 days after the M7.0 earthquake and in the range of 10° latitude by 10° longitude centered on an M7.0 epicenter. Panels (**a**–**c**) show the residual magnetic field in radial, azimuthal and parallel directions. Blue stars on *x*-axes represent the epicenter's latitude. *y*-axis indicates time-differences (ΔT in days) between Swarm observations and the earthquake time.

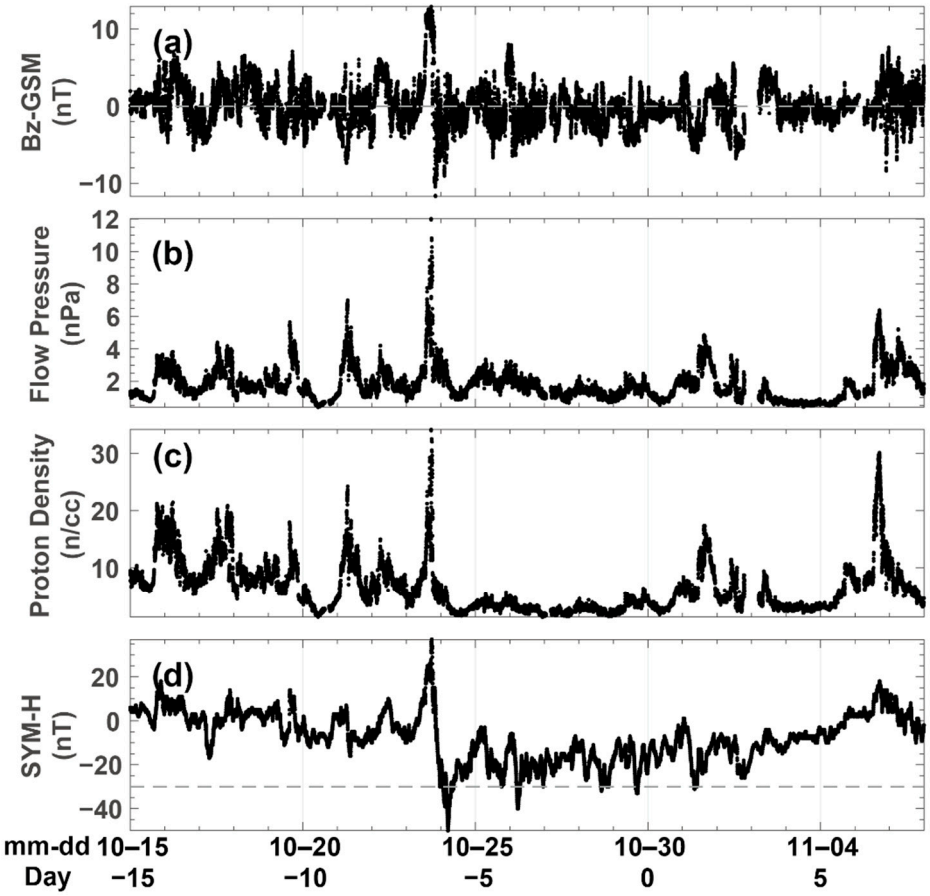

Figure 9. Solar wind parameters and SYM-H indices from 15 October to 6 November, i.e., 15 days before to 7 days after the M7.0 earthquake. (**a**) IMF Bz in GSM coordinates; (**b**) the solar wind dynamic pressure; (**c**) the solar wind proton density and (**d**) the SYM-H index. The dashed line indicates −30 nT.

4. Discussion

This work analyzes the magnetic disturbances related to interplate and intraplate earthquakes recorded by Swarm satellites. Magnetic disturbances associated with the interplate shallow earthquake (M7.7) have larger amplitudes than those related to the intraplate shallow earthquake (M7.0). In this paper, we propose a new method for analyzing magnetic disturbances possibly related to earthquakes. With our method, we try to eliminate already-known factors that can cause magnetic effects. The most common approach is to check solar wind parameters and geomagnetic indices to exclude the influences of space weather events. In addition, magnetic signatures of equatorial plasma depletions (EPDs) and midlatitude magnetic fluctuations are investigated by jointly analyzing electron density (Ne) and field-aligned currents (FACs).

Magnetic field variations in this work are observed in the nightside (LT~17/18~02). Previous studies have shown magnetic perturbations related to postsunset equatorial plasma depletions. Their occurrence rate is the lowest at 18 LT and very low at 02 LT. The highest is between 21 and 22 LT [23]. These magnetic field fluctuations are caused by two types of currents: diamagnetic currents flowing across the depletions, producing magnetic perturbations parallel to the ambient field and field-aligned currents (FACs) flowing within the edges of the depletions, generating transverse magnetic field perturbations [24,25]. From Figures 1 and 8, we know that the magnetic field fluctuates in perpendicular components. Figures 3 and 4 present transverse magnetic perturbations and simultaneous Ne. There are no Ne depletions shown in Figures 3d and 4d. Residual Ne disturbances with a scale of 10^3 cm^{-3} on day -11 can be seen in Figure 4e. It is much weaker than the

density change of at least 10^5 cm^{-3} to generate a detectable magnetic signal [23,26]. Similar changes of Ne in Figure A2 are presented. These features in Ne suggest that there is no clear relationship between equatorial plasma depletions and magnetic disturbances.

Another influence comes from midlatitude magnetic fluctuations (MMFs) [26]. Nighttime medium-scale MMFs have been related to nighttime medium-scale traveling ionospheric disturbances (MSTIDs) [27]. Their work interprets MMFs in terms of FACs, and most estimated FACs have amplitudes of approximately 0.15 $\mu A/m^2$. Small-scale MMFs (<10 km) at midlatitudes and low latitudes are explained as narrow, intense interhemispheric FACs with several $\mu A/m^2$ [28]. FACs in the vicinity of the epicenter in Figures 5 and A3 are very weak, almost around the background FACs indicated by red dashed lines, which are in a similar amplitude as given by [21]. Although magnetic perturbations in this work are in perpendicular magnetic field components, they are not significantly affected by enhanced interhemispheric FACs.

5. Conclusions

This paper presents interplate and intraplate earthquake case studies to demonstrate the elimination of some known magnetic disturbances induced by non-earthquake sources. We present magnetic disturbances around earthquakes recorded by Swarm satellites. By correlating these magnetic disturbances with space weather events, equatorial plasma depletions and midlatitude magnetic fluctuations, we found that magnetic disturbances several days before earthquakes do not show clear associations with already known non-earthquake disturbances. These magnetic disturbances possibly related to earthquakes oscillate below 2 Hz in the transverse magnetic field, propagating along the background magnetic field and mostly linearly polarized.

The method proposed in this study can be used in the daily practice of analyzing earthquake precursors by using magnetic data observed by satellites. Further work could conduct to categorize different magnetic disturbances and deepen the understanding of their origins. For magnetic disturbances possibly related to earthquakes observed by satellites, combining geomagnetic data to discuss and study correlations between magnetic disturbances and earthquakes in different seismotectonic circumstances is also needed in future research.

Author Contributions: Conceptualization, X.-Y.O.; funding acquisition, X.-Y.O.; investigation, X.-Y.O.; methodology, X.-Y.O.; visualization, X.-Y.O. and Y.-F.W.; writing—original draft, X.-Y.O.; writing—review and editing, Y.-F.W., X.-M.Z., Y.-L.W. and Y.-Y.W. All authors have read and agreed to the published version of the manuscript.

Funding: This research was funded by the APSCO, dragon 5 cooperation proposal and the National Key R&D Program of China, grant number "the APSCO Earthquake Research Project Phase II, #59308 and 2018YFC1503506". Yong-Fu Wang is supported by the Innovation Fund from Joint Innovation Center of Space Science (Aerospace Shanghai).

Data Availability Statement: The Swarm data can be accessed at https://earth.esa.int/swarm (accessed on 20 December 2021). The solar wind and geomagnetic activity data can be acquired from the OMNIWeb service at https://omniweb.gsfc.nasa.gov (accessed on 22 December 2021). The earthquake information is available at https://earthquake.usgs.gov/earthquakes/search (accessed on 10 December 2021).

Acknowledgments: The authors would like to thank Hui Wang (Wuhan University), Yueren Xu, Lianqing Zhou and Qi Liu (IEF, CEA) for helpful discussions.

Conflicts of Interest: The authors declare no conflict of interest.

Appendix A

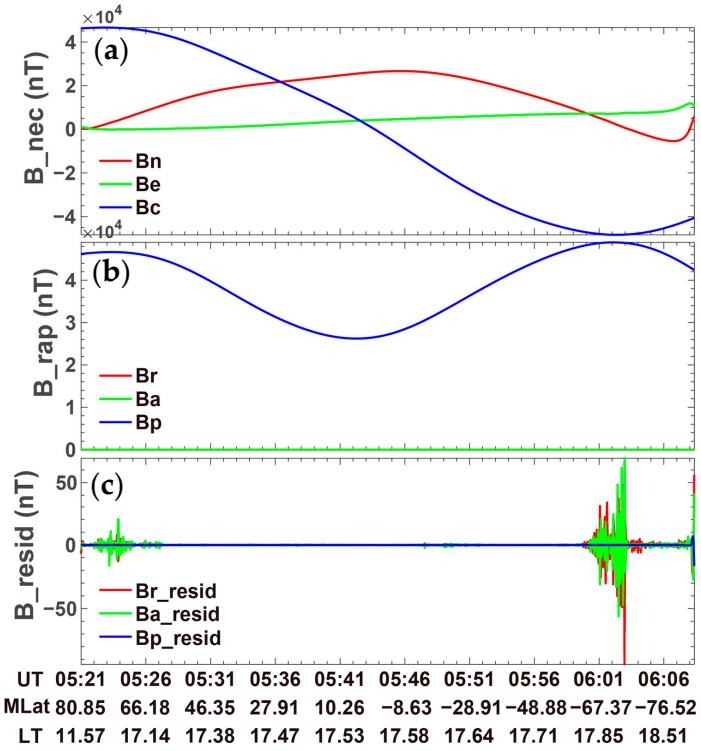

Figure A1. (**a**) Three magnetic field components in North-East-Center (NEC) coordinates; (**b**) three magnetic field components in local field-aligned coordinates; (**c**) residual magnetic field in local field-aligned coordinates.

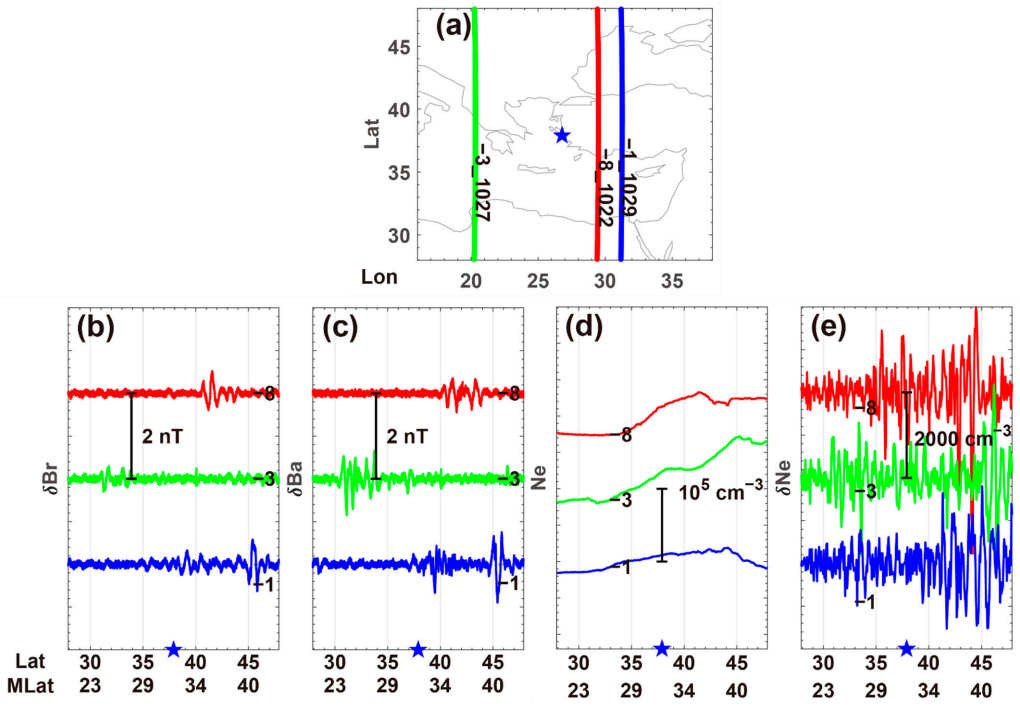

Figure A2. Remaining magnetic disturbances (LT~02) after removing the main influences of space weather events. (**a**) Swarm B orbits with magnetic disturbances in the range of 10° latitude by 10° longitude centered on the M7.0 earthquake. Annotations in panel (**a**) show time differences (ΔT in days) and dates (mmdd) of each orbit; (**b**,**c**) present the residual magnetic field in Br and Ba components; (**d**) original Ne; and (**e**) residual Ne. The blue star indicates the epicenter.

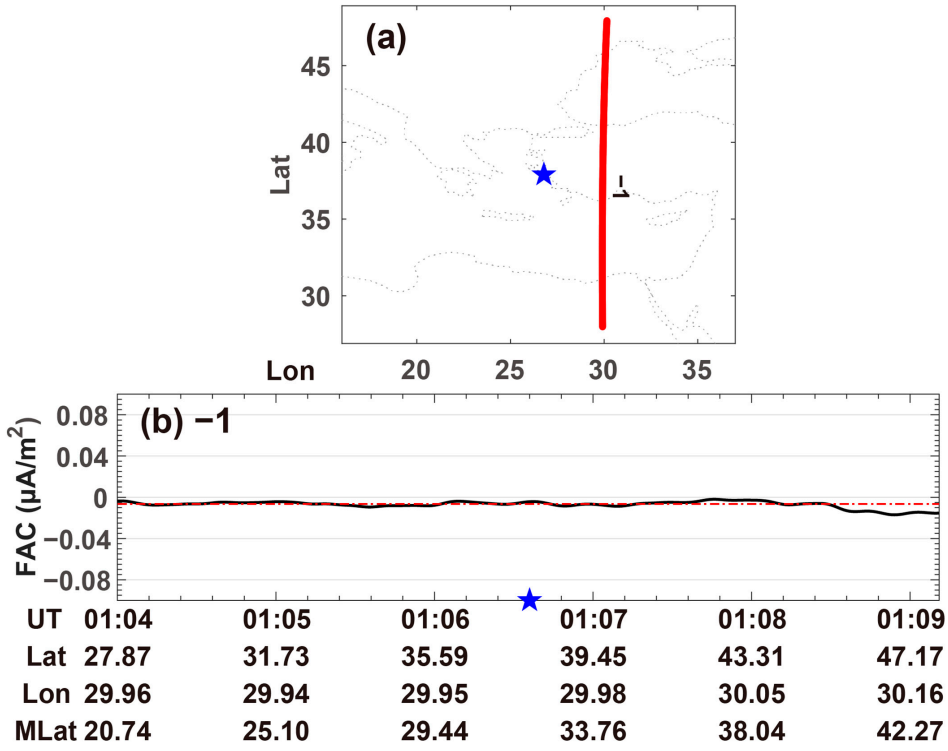

Figure A3. Field-aligned currents (LT~03) derived from the Swarm A and C pair in the range of 10° latitude by 10° longitude centered on the M7.0 earthquake. There is no FAC data at ΔT = −8 and −3 days. (**a**) Orbits on ΔT = −1 day, blue star indicates the epicenter; (**b**) FACs along orbits on day −1, and blue star shows the epicenter's latitude.

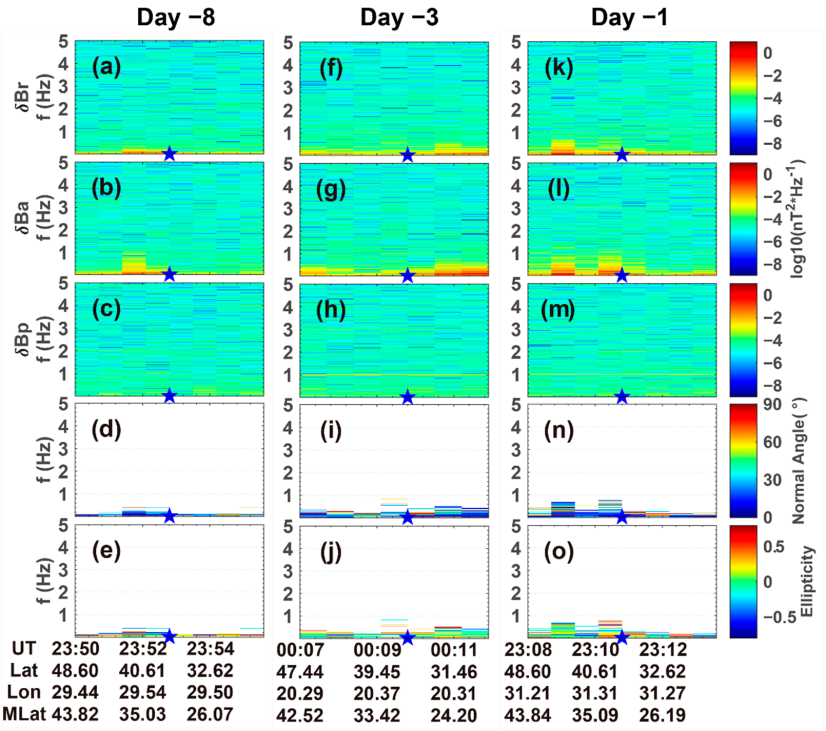

Figure A4. Power spectral density and polarization parameters of disturbed orbits at ΔT = −8, −3 and −1 days. For example, (**a**–**c**) show the power spectral density of Br, Ba and Bp components at ΔT = −8 days; (**d**,**e**) present wave normal angle and ellipticity at ΔT = −8 days. The second and third columns (**f**–**o**) display results at ΔT = −3 and −1 days. The blue star indicates the epicenter.

References

1. Zhao, S.; Shen, X.; Liao, L.; Zhima, Z.; Zhou, C.; Wang, Z.; Cui, J.; Lu, H. Investigation of Precursors in VLF Subionospheric Signals Related to Strong Earthquakes (M > 7) in Western China and Possible Explanations. *Remote Sens.* **2020**, *12*, 3563. [CrossRef]
2. Zhang, X.; Wang, Y.; Boudjada, M.Y.; Liu, J.; Magnes, W.; Zhou, Y.; Du, X. Multi-Experiment Observations of Ionospheric Disturbances as Precursory Effects of the Indonesian Ms6.9 Earthquake on 5 August 2018. *Remote Sens.* **2020**, *12*, 4050. [CrossRef]
3. Yumoto, K.; Ikemoto, S.; Cardinal, M.G.; Hayakawa, M.; Hattori, K.; Liu, J.Y.; Saroso, S.; Ruhimat, M.; Husni, M.; Widarto, D.; et al. A new ULF wave analysis for Seismo-Electromagnetics using CPMN/MAGDAS data. *Phys. Chem. Earth Parts A B C* **2009**, *34*, 360–366. [CrossRef]
4. Fraser-Smith, A.C.; Bernardi, A.; McGill, P.R.; Ladd, M.E.; Helliwell, R.A.; Villard, O.G. Low-frequency magnetic field measurements near the epicenter of the Ms 7.1 Loma Prieta earthquake. *Geophys. Res. Lett.* **1990**, *17*, 1465–1468. [CrossRef]
5. Hayakawa, M.; Kawate, R.; Molchanov, O.A.; Yumoto, K. Results of ultra-low-frequency magnetic field measurements during the Guam Earthquake of 8 August 1993. *Geophys. Res. Lett.* **1996**, *23*, 241–244. [CrossRef]
6. Bortnik, J.; Cutler, J.W.; Dunson, C.; Bleier, T.E. The possible statistical relation of Pc1 pulsations to Earthquake occurrence at low latitudes. *Ann. Geophys.* **2008**, *26*, 2825–2836. [CrossRef]
7. Han, P.; Hattori, K.; Hirokawa, M.; Zhuang, J.; Chen, C.-H.; Febriani, F.; Yamaguchi, H.; Yoshino, C.; Liu, J.-Y.; Yoshida, S. Statistical analysis of ULF seismomagnetic phenomena at Kakioka, Japan, during 2001–2010. *J. Geophys. Res. Space Phys.* **2014**, *119*, 4998–5011. [CrossRef]
8. Hattori, K.; Han, P.; Yoshino, C.; Febriani, F.; Yamaguchi, H.; Chen, C.-H. Investigation of ULF Seismo-Magnetic Phenomena in Kanto, Japan During 2000–2010: Case Studies and Statistical Studies. *Surv. Geophys.* **2013**, *34*, 293–316. [CrossRef]
9. Molchanov, O.; Hayakawa, M.; Rafalsky, V. Penetration characteristics of electromagnetic emissions from an underground seismic source into the atmosphere, ionosphere, and magnetosphere. *J. Geophys. Res. Space Phys.* **1995**, *100*, 1691–1712. [CrossRef]
10. Athanasiou, M.A.; Anagnostopoulos, G.C.; Iliopoulos, A.C.; Pavlos, G.P.; David, C.N. Enhanced ULF radiation observed by DEMETER two months around the strong 2010 Haiti earthquake. *Nat. Hazards Earth Syst. Sci.* **2011**, *11*, 1091–1098. [CrossRef]
11. Walker, S.N.; Kadirkamanathan, V.; Pokhotelov, O.A. Changes in the ultra-low frequency wave field during the precursor phase to the Sichuan earthquake: DEMETER observations. *Ann. Geophys.* **2013**, *31*, 1597–1603. [CrossRef]
12. Zhang, X.; Chen, H.; Liu, J.; Shen, X.; Miao, Y.; Du, X.; Qian, J. Ground-based and satellite DC-ULF electric field anomalies around Wenchuan M8.0 earthquake. *Adv. Space Res.* **2012**, *50*, 85–95. [CrossRef]
13. De Santis, A.; Balasis, G.; Pavón-Carrasco, F.J.; Cianchini, G.; Mandea, M. Potential earthquake precursory pattern from space: The 2015 Nepal event as seen by magnetic Swarm satellites. *Earth Planet. Sci. Lett.* **2017**, *461*, 119–126. [CrossRef]
14. Ouyang, X.Y.; Parrot, M.; Bortnik, J. ULF Wave Activity Observed in the Nighttime Ionosphere Above and Some Hours Before Strong Earthquakes. *J. Geophys. Res. Space Phys.* **2020**, *125*, e2020JA028396. [CrossRef]
15. Berthelier, J.J.; Godefroy, M.; Leblanc, F.; Malingre, M.; Menvielle, M.; Lagoutte, D.; Brochot, J.Y.; Colin, F.; Elie, F.; Legendre, C. ICE, the electric field experiment on DEMETER. *Planet. Space Sci.* **2006**, *54*, 456–471. [CrossRef]
16. Savitzky, A.; Golay, M.J.E. Smoothing and Differentiation of Data by Simplified Least Squares Procedures. *Anal. Chem.* **1964**, *36*, 1627–1639. [CrossRef]
17. Kim, H.; Hwang, J.; Park, J.; Miyashita, Y.; Shiokawa, K.; Mann, I.R.; Raita, T.; Lee, J. Large-Scale Ducting of Pc1 Pulsations Observed by Swarm Satellites and Multiple Ground Networks. *Geophys. Res. Lett.* **2018**, *45*, 12–703. [CrossRef]
18. Means, J.D. Use of the three-dimensional covariance matrix in analyzing the polarization properties of plane waves. *J. Geophys. Res.* **1972**, *77*, 5551–5559. [CrossRef]
19. Bortnik, J.; Cutler, J.W.; Dunson, C.; Bleier, T.E. An automatic wave detection algorithm applied to Pc1 pulsations. *J. Geophys. Res. Space Phys.* **2007**, *112*, A04204. [CrossRef]
20. Dobrovolsky, I.P.; Zubkov, S.I.; Miachkin, V.I. Estimation of the size of earthquake preparation zones. *Pure Appl. Geophys.* **1979**, *117*, 1025–1044. [CrossRef]
21. Lühr, H.; Kervalishvili, G.; Michaelis, I.; Rauberg, J.; Ritter, P.; Park, J.; Merayo, J.M.G.; Brauer, P. The interhemispheric and F region dynamo currents revisited with the Swarm constellation. *Geophys. Res. Lett.* **2015**, *42*, 3069–3075. [CrossRef]
22. Ritter, P.; Lühr, H.; Rauberg, J. Determining field-aligned currents with the Swarm constellation mission. *Earth Planets Space* **2013**, *65*, 9. [CrossRef]
23. Stolle, C.; Lühr, H.; Rother, M.; Balasis, G. Magnetic signatures of equatorial spread F as observed by the CHAMP satellite. *J. Geophys. Res. Space Phys.* **2006**, *111*, A02304. [CrossRef]
24. Rodríguez-Zuluaga, J.; Stolle, C.; Park, J. On the direction of the Poynting flux associated with equatorial plasma depletions as derived from Swarm. *Geophys. Res. Lett.* **2017**, *44*, 5884–5891. [CrossRef]
25. Rodríguez-Zuluaga, J.; Stolle, C.; Yamazaki, Y.; Lühr, H.; Park, J.; Scherliess, L.; Chau, J.L. On the Balance Between Plasma and Magnetic Pressure Across Equatorial Plasma Depletions. *J. Geophys. Res. Space Phys.* **2019**, *124*, 5936–5944. [CrossRef]
26. Yokoyama, T.; Stolle, C. Low and Midlatitude Ionospheric Plasma Density Irregularities and Their Effects on Geomagnetic Field. *Space Sci Rev.* **2017**, *206*, 495–519. [CrossRef]

27. Park, J.; Lühr, H.; Stolle, C.; Rother, M.; Min, K.W.; Chung, J.-K.; Kim, Y.H.; Michaelis, I.; Noja, M. Magnetic signatures of medium-scale traveling ionospheric disturbances as observed by CHAMP. *J. Geophys. Res. Space Phys.* **2009**, *114*, A03307. [CrossRef]
28. Yin, F.; Lühr, H.; Park, J.; Wang, L. Comprehensive Analysis of the Magnetic Signatures of Small-Scale Traveling Ionospheric Disturbances, as Observed by Swarm. *J. Geophys. Res. Space Phys.* **2019**, *124*, 10794–10815. [CrossRef]